IV International Conference on Particle-based Methods – Fundamentals and Applications
PARTICLES 2015
E. Oñate, M. Bischoff, D.R.J. Owen, P. Wriggers & T. Zohdi (Eds)

HYDRO-MECHANICAL CONTINUUM MODELLING OF AN EXPERIMENTAL SLOPE WITH A MATERIAL STABILITY CRITERION

EVANTHIA KAKOGIANNOU[1], MARCO LORA[1] AND LORENZO SANAVIA[1]

[1]Department of Civil, Architectural and Environmental Engineering (DICEA)
University of Padua (UNIPD)
Via F. Marzolo 9, 35131 Padua, Italy
evanthia.kakogiannou@unipd.it, marco.lora@dicea.unipd.it, lorenzo.sanavia@unipd.it
web page: http://www.dicea.unipd.it

Key words: Landslides, Infiltration process, Multiphysics problems, Variably saturated porous media, Second order work criterion.

Abstract. In the case of hydrologically driven slope instability, the behaviour of the variably saturated soil is closely related not only to the distribution of pore-water pressure, but also to the stress state during rainfall infiltration. This phenomenon involves both mechanical and hydrological processes. The aim of the scientific community focuses on the development of powerful models capable of a reliable prediction of the landslide initiation. Multiphysics numerical modelling approaches can account for these complex processes including increased saturation, fluid flow and inelastic solid deformation. To this end, a physics based framework is presented in this work for the continuum modelling of an experimental slope subjected to rainfall infiltration. The failure mechanism is assessed, also by the use of the second order work criterion. The rainfall induced deformation is quantified and the evolution of the pore water pressure is compared with the in situ measurements.

1 INTRODUCTION

Hydrologically-driven slope instability represents a major threat to human life and property. Due to the usual large extension of rainfall events this type of slope failure can be triggered over large areas and generally involves shallow soil deposit of different grading and origin [1]. Considering the destructiveness of these landslides, the understanding and the hydro-mechanical modelling of the mechanisms occurring inside the source areas are a fundamental issue for the mitigation of the posed risk to life and facilities.

The most common approach for the numerical modelling of rainfall induced slope failure in engineering practice is to uncouple the fluid flow and slope stability problems and treat them in a sequential fashion. In this sense, a seepage analysis (assuming a rigid solid skeleton) is performed first for the calculation of the water pressure distribution, which is then followed by a limit equilibrium analysis for the slope stability problem.

However, the behaviour of a soil slope under rainfall conditions is closely related not only to the distribution of pore-water pressure but also to the stress state during infiltration. More realistic solutions to the coupled governing equations for deformation and seepage should be obtained when the soil of the slope are considered as deformable and in variably saturated

conditions. For this reason, in this work, the modelling of rainfall induced landslides is considered as a coupled variably saturated hydro-mechanical problem. In order to examine this argument, a hydro-mechanical analysis of a large scale slope stability experimental test, subjected to rainfall infiltration, is presented in this paper; for the numerical simulation the geometrically linear finite element code Comes-Geo [2], [3] for non-isothermal elasto-plastic multiphase solid porous materials as developed by [4], [5], [6] is used.

Furthermore, a recently proposed criterion for instability, the second order work criterion, based on Hill's sufficient condition of stability [7] is implemented on the abovementioned code. It is based on studying the sign of the second order work at the material point level and it is used in this analysis for the detection of the onset of the failure.

In the following, the mathematical model for non-isothermal multiphase porous materials is summarised first. Then the definition of the second order work criterion is reviewed. Finally the results of the hydro-mechanical analysis are presented and discussed.

2 MATHEMATICAL MODEL

The mathematical model necessary to simulate the thermo-hydro-mechanical transient behaviour of fully and partially saturated porous media is developed in [4] following the works by [2] and [8] and using averaging theories by [9], [10]. For sake of brevity, only a summary of the underlying physical model is presented here. For the complete description of the model from its mathematical formulation to the numerical implementation, the reader can refer to the abovementioned works of the authors.

The geomaterial is considered as a variably saturated porous medium and is treated as a multiphase system composed of a solid skeleton (*s*) with open pores filled with liquid water (*w*) and gas (*g*). All constituents are assumed to be immiscible and chemically non-reacting, except for the gas which is assumed to behave as an ideal mixture of dry air (non-condensable gas, *ga*) and water vapour (condensable one, *gw*).In the model, heat conduction, vapour diffusion, heat convection, water flow due to pressure gradients or capillary effects and water phase change (evaporation and condensation) inside the pores are taken into account. All fluids are in contact with the solid phase and the solid is deformable resulting in coupling of the fluid, the solid and the thermal effects.

The final model consists of four balance equations: mass balance of the dry air, mass balance of the water species (both liquid and vapour, phase change is taken into account), enthalpy of the whole medium (latent heat of the phase change is considered) and the equilibrium equations of the multiphase medium. They are completed with an appropriate set of constitutive and state equations, as well as some thermo-dynamic relationships.

The governing equations of the model, are expressed in terms of the chosen state variables: gas pressure p^g, capillary pressure $p^c = p^g - p^w$ (p^w is the water pressure), temperature T and the displacement vector of the solid matrix $\mathbf{u}$.

2.1 Macroscopic Balance Equations

The macroscopic equations of the model are now summarized [3], [4] .These equations are obtained introducing the following assumptions in the model:

- at the micro-level the porous medium is assumed to be constituted of incompressible solid and water constituents, while gas is considered compressible

- the process is considered as quasi-static and is developed in the geometrically linear framework.

The equilibrium equations of the mixture in terms of generalized Cauchy effective stress $\boldsymbol{\sigma}'(\mathbf{x},t)$, assume the form:

$$div\left(\boldsymbol{\sigma}'-\left[p^g - S^w p^c\right]\mathbf{1}\right)+\rho\mathbf{g}=0 \tag{1}$$

where $\rho(\mathbf{x},t)$ is the density of the mixture, $\rho=\left[1-n\right]\rho^s+nS_w\rho^w+nS_g\rho^g$ with $n(\mathbf{x},t)$ the porosity, $S_w(\mathbf{x},t)$ and $S_g(\mathbf{x},t)$ the liquid water and gas degree of saturation, respectively and $\mathbf{1}$ is the second order identity tensor.

The mass balance equation for the solid phase, the liquid water and the water vapour is:

$$\begin{aligned}
&n\left[\rho^w-\rho^{gw}\right]\left[\frac{\partial S_w}{\partial t}\right]+\left[\rho^w S_w-\rho^{gw}\left[1-S_w\right]\right]div\left(\frac{\partial\mathbf{u}}{\partial t}\right)\\
&+\left[1-S_w\right]n\frac{\partial\rho^{gw}}{\partial t}-div\left(\rho^g\frac{M_\alpha M_w}{M_g^2}\mathbf{D}_g^{gw}grad\left(\frac{\partial p^{gw}}{\partial p^g}\right)\right)\\
&+div\left(\rho^w\frac{\mathbf{k}k^{rw}}{\mu^w}\left[-grad(p^g)+grad(p^c)+\rho^w\mathbf{g}\right]\right)\\
&+div\left(\rho^{gw}\frac{\mathbf{k}k^{rg}}{\mu^g}\left[-grad(p^g)+\rho^w\mathbf{g}\right]\right)-\beta_{swg}\frac{\partial T}{\partial t}=0
\end{aligned} \tag{2}$$

where $\rho^{gw}(\mathbf{x},t)$ is the microscopic mass density of the water vapour, $\mathbf{k}\left(\mathbf{x},t\right)=\mathbf{K}_w\mu^w/(\rho^w g)$ is the intrinsic permeability tensor of the porous matrix in saturated condition [m^2], with $\mathbf{K}_w(\mathbf{x},t)$ the hydraulic conductivity tensor [m/s] and $\mathbf{g}$ the gravity acceleration value. $k^{rw}(\mathbf{x},t)$ is the water relative permeability parameter and $\mu^w(\mathbf{x},t)$, the dynamic viscosity of liquid water, function of the temperature, $T(\mathbf{x},t)$. Similarly, $k^{rg}(\mathbf{x},t)$ is the gas relative permeability parameter and $\mu^g(\mathbf{x},t)$ the dynamic viscosity of gas; $\beta_{swg}(\mathbf{x},t)$ is the cubic thermal expansion coefficient; $\mathbf{D}_g^{gw}(\mathbf{x})$ is the effective diffusivity tensor of water vapour (the diffusing phase) in the gas phase (the phase in which diffusion takes place) contained in the pore space, function of the tortuosity factor, and M_a, M_w and $M_g(\mathbf{x},t)$ the molar mass of dry air, liquid water and gas mixture, respectively. In order to account for the diffusive – dispersive flux of the vapour in the gas phase Fick's law is used, while advective flows are modelled with Darcy's law.

The mass balance equation for dry air is:

$$n\rho^{g\alpha}\left[\frac{\partial S_w}{\partial t}\right]+\rho^{g\alpha}\left[1-S_w\right]div\left(\frac{\partial \mathbf{u}}{\partial t}\right)+nS_g\frac{\partial \rho^{g\alpha}}{\partial t}-div\left(\rho^g\frac{M_\alpha M_w}{M_g^2}\mathbf{D}_g^{g\alpha}grad\left(\frac{\partial p^{g\alpha}}{\partial p^g}\right)\right.$$
$$\left.+div\left(\rho^{g\alpha}\frac{\mathbf{k}k^{rg}}{\mu^g}\left[-grad(p^g)+\rho^g\mathbf{g}\right]\right)-\beta_{swg}\rho^{g\alpha}\left[1-n\right]\left[1-S_w\right]\frac{\partial T}{\partial t}=0\right. \tag{3}$$

where, similarly, $\rho^{ga}(\mathbf{x},t)$ is the microscopic mass density of the dry air, $\mathbf{D}_g^{ga}(\mathbf{x})$ is the effective diffusivity tensor of dry air in the gas phase contained in the pore space. Equations (2), (3) include the mass balance equation for the solid phase:

$$\frac{\partial n}{\partial t}=\left[1-n\right]div\left(\frac{\partial u}{\partial t}\right)-\left[1-n\right]\beta_s\frac{\partial T}{\partial t} \tag{4}$$

The enthalpy balance equation of the mixture is:

$$\left(\rho C_p\right)_{eff}\frac{\partial T}{\partial t}+\rho^w C_p^w\left(\frac{\mathbf{k}k^{rw}}{\mu^w}\left[-grad(p^g)+grad(p^c)+\rho^w\mathbf{g}\right]\right)\cdot grad(T)$$
$$+\rho^g C_p^g\left(\frac{\mathbf{k}k^{rg}}{\mu^g}\left[-grad(p^g)+\rho^g\mathbf{g}\right]\right)\cdot grad(T)-div\left(\chi_{eff}grad(T)\right)=-\dot{m}_{vap}\Delta H_{vap} \tag{5}$$

where, $\left(\rho C_p\right)_{eff}$ is the effective thermal capacity of the porous medium, $\rho^w C_p^w$ and $\rho^g C_p^g$ are the specific heat of the water and gas mixture respectively, χ_{eff} the effective thermal conductivity of the porous medium and the right hand side term considers the contribution of the evaporation and condensation. This balance equation takes into account the heat transfer through conduction and convection as well as latent heat transfer and neglects the terms related to the mechanical work induced by density variations due to temperature changes of the phases and induced by volume fraction changes [2].

2.2 Constitutive relations

The mechanical behaviour of the soil skeleton is described within the elasto-plastic constitutive framework. For the simulations analyzed in this report, the Drucker-Prager yield surface with isotropic linear hardening behaviour and non-associated plastic flow [4] is used for simplicity:

$$F\left(p',\mathbf{s}',\xi\right)=3\alpha_F p'+\left\|\mathbf{s}'\right\|-\beta_F\sqrt{\frac{2}{3}}\left[c_0+h\xi\right] \tag{6}$$

in which $p'=\frac{1}{3}\left[\boldsymbol{\sigma}':\mathbf{1}\right]$ is the mean effective Cauchy stress tensor, $\left\|\mathbf{s}'\right\|$ is the norm of the deviator effective Cauchy stress tensor $\boldsymbol{\sigma}'$, c_0 is the apparent cohesion, α_F and β_F are two material parameters related to the friction angle φ of the soil

$$\alpha_F = 2\frac{\sqrt{\frac{2}{3}}\sin\varphi}{3-\sin\varphi} \qquad \beta_F = 2\frac{6\cos\varphi}{3-\sin\varphi} \tag{7}$$

and h and ξ the hardening/softening modulus and the equivalent plastic strain variable, respectively.

For the gaseous mixture which is assumed to be a perfect mixture of two ideal gases (dry air and water vapour) the ideal gas law is introduced. The equation of state of perfect gas (the Clapeyron equation) and Dalton's law are applied to dry air (*ga*), water vapour (*gw*) and moist air (*g*). In the partially saturated zones, the water vapour pressure $p^{gw}(\mathbf{x},t)$ is obtained from the Kelvin-Laplace equation. The saturation $S_\pi(\mathbf{x},t)$ and the relative permeability $k^{r\pi}(\mathbf{x},t)$ are experimentally determined functions of the capillary pressure and the temperature.

4 FINITE ELEMENT FORMULATION

The governing equations of the problem are discretized in space by means of the finite element method. Their discretized form is obtained by means of the Bubnov-Galerkin method for the discretization in space. The time discretization is accomplished through a fully implicit finite difference scheme. Because of the non-linearity of the system of equations the solution is obtained with a Newton-Rapshon type procedure. Details concerning the matrices and the residuum vector of the linearized equations system of the finite element model can be found in [4].

5 SECOND ORDER WORK MATERIAL INSTABILITY CRITERION

Although the notion of failure in soils (or more generally geomaterials) was long described as a perfect plastic limit, it has been observed in practice that failure can occur well before the Mohr-Coulomb criterion is met. This is due to the non-associated behaviour (the yield surface does not coincide with the plastic potential) of frictional materials, such as soils. According to [11], [12] in case of such materials, one can find an unstable domain strictly inside the plastic limit envelope. What is more, material instabilities can lead to diffuse modes of failure inside the plastic limit condition, which are characterized by the lack of localization patterns and for this reason cannot be detected neither by a plastic limit criterion nor by a localization criterion [13], [14]. A characteristic example of this kind of failure can be illustrated through an undrained test on loose sand. If a small additional force is applied at the stress peak value, a sudden failure occurs with no localisation pattern strictly inside the Mohr-Coulomb plastic limit condition.

Hill's sufficient condition of stability [7], which is based on the sign of second-order work, seems to be a pertinent stability criterion to detect these diffuse modes of failure [15], according to which a mechanical stress–strain state is considered as stable if, for any couple $(d\boldsymbol{\sigma}, d\boldsymbol{\varepsilon})$ linked by the rate-dependent constitutive relation (stiffness tensor: $\boldsymbol{M}$) the second order work W_2 is strictly positive:

$$\forall (d\boldsymbol{\sigma}, d\boldsymbol{\varepsilon}) \in \mathrm{R}^{2n} \setminus \{0\} \text{ with } d\boldsymbol{\varepsilon} = \boldsymbol{M} : d\boldsymbol{\sigma},\ W_2 = d\boldsymbol{\sigma} : d\boldsymbol{\varepsilon} > 0 \tag{8}$$

where n is the dimension of the stress space. Otherwise, if the scalar product is zero or negative then the material point is found on a potentially unstable state.

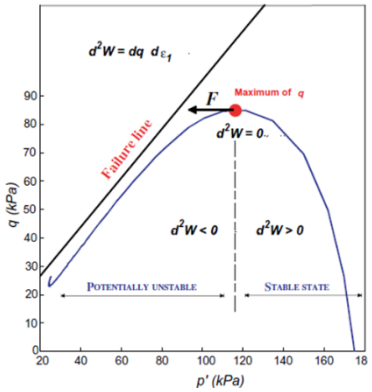

Figure 1: Typical triaxial behaviour of a loose sand [13].

As illustrated in Figure 1, the transition from the stable to the unstable regime can be detected by the sign of the second order work criterion.

6 NUMERICAL SIMULATION OF AN UNSATURATED SOIL SLOPE SUBJECTED TO RAINFALL INFILTRATION

6.1 Description of the experiment and the numerical modelisation

The experiment which was carried out in the University of Padua [16],[17],[18] reproduces a stability problem of a large-scale slope due to rain infiltration.

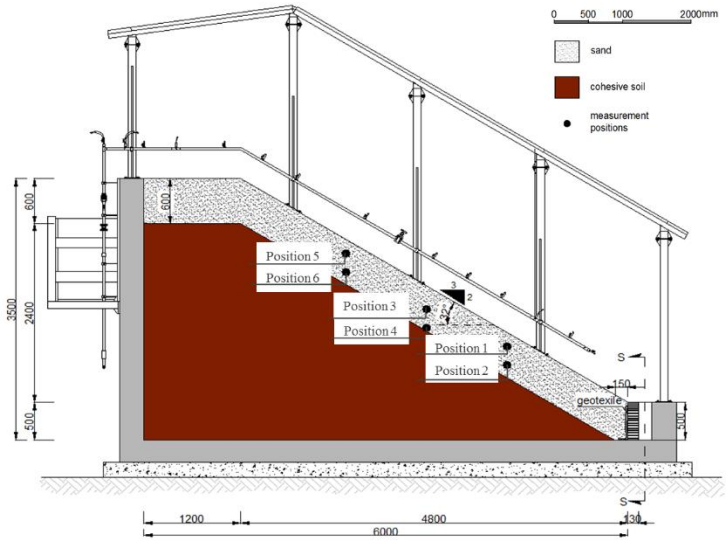

Figure 2: Geometry and stratigraphy of the slope (longitudinal section) and representation of the measurement positions [16], [17] .

To this end, a steady rainfall intensity equal to 150mm/h is applied until the mobilization of the soil. The slope consists of two soil layers: a shallow permeable layer of loose sand

overlying a dense clayey soil substratum. The height varies linearly from 3.5m to 0.5m, such that a sloping angle of 32° can be assigned to the soil. The dimensions of the model and the stratigraphy are presented in Figure 2. The values of the mechanical and hydraulic properties of the each material layer, which were used in the computation, are presented on Table 1.

Table 1: Soil parameters used in the computation

Definition	Label	Loose Sand	Clay
Density	ρ^s [kg/m^3]	2718	2680
Friction angle	φ[°]	34.0	22.0
Cohesion	c [Pa]	1.0E+03	1.0E+04
Initial Young modulus	E [Pa]	2.5E+06	1.0E+07
Poisson's ratio	ν [-]	0.3	0.3
Angle of dilatancy	ψ[°]	0	4
Hardening modulus	h [Pa]	4.8E+03	0.0
Intrinsic Permeability	k [m^2]	2.091E-11	2.98E-13
Initial porosity	n [-]	0.569	0.384

The estimates of the retention functions for the loose sand layer were inferred by fitting the retention tests data as well as by an inverse modelling, applied to the measurements data which were obtained from the landslide test. The curves (the continuous and dashed black lines in Figure 3) were obtained in accordance to the Brooks and Corey [19] and van Genuchten [20] models.

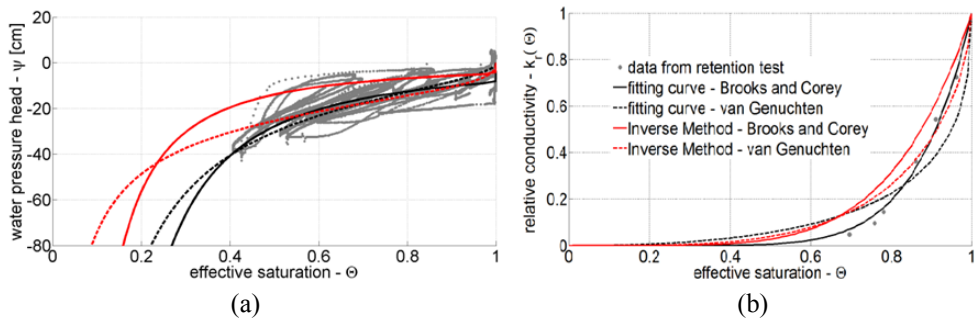

(a) (b)

Figure 3: Retention curves of the loose sand layer: (a) the relation of the effective saturation with the pressure head; (b) the relation of the relative conductivity with the effective saturation [16], [17].

The Brooks and Corey [19] model appeared to approach better the field data especially in terms of water pressure head and therefore it was the expression that was implemented on the numerical code:

$$\Theta = \left(\frac{h}{h_b}\right)^{-\lambda} \quad \text{and} \quad K(\Theta) = \mathrm{K}_S \cdot \Theta^{\frac{2}{\lambda}+l+2} \quad \text{if } h < h_b \tag{9}$$

where $\Theta = \frac{\theta - \theta_r}{\theta_s - \theta_r}$ is the effective saturation, with θ_r and θ_s the residual and the saturated volumetric water content respectively; h is the water pressure head and h_b the bubbling pressure; $K(\Theta)$ and K_S are the hydraulic conductivity in partially saturated conditions, respectively; λ and l are shape parameters.

Regarding the clayey layer, the only measured hydraulic parameter was the hydraulic conductivity in saturated conditions. Other unknown parameters concerning the retention curves are assigned from the literature [21].

In Figure 4 the mesh which has been created, is presented along with the initial and boundary conditions applied to the slope. The finite element mesh is composed of 468 eight-noded quadratic quadrilateral elements. Vertical and horizontal displacements are constrained at the bottom and horizontal displacements at the lateral surfaces. Initially, the stress state is computed in equilibrium with the gravity load and the initial hydro-thermal conditions (Figure 4). The stress state and the state variables calculated by this first analysis form the initial conditions for the successive run. Subsequently, rainfall infiltration is simulated by means of an imposed boundary flux of 150mm/hr along the upper surface (the rain input has the real value as this that was applied during the experiment). When the toe of the slope saturates, an outflow is distributed along its vertical side, with a value equal to the one that was measured in situ at the moment of the failure, as a first approximation.

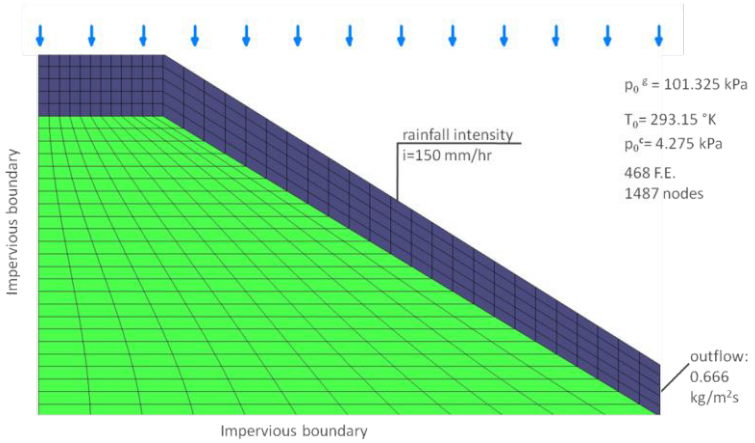

Figure 4: Description of the discretization of the slope, initial and boundary conditions.

6.2 Results and discussion

After 1.8 hr of the applied rainfall, the numerical solution became unstable and the numerical convergence was lost. This was also the actual time failure of the field experiment. Figure 5 illustrates the contours of degree of saturation nearly at the beginning of the simulation and after 1.8hr, when the convergence of the norm of displacements cannot be achieved any further. In more detail, in figure 5a can be observed the procedure of rainfall infiltration: a wetting front percolating vertically downwards, across the sand layer. The wetting front does not saturate the sand in this case as the infiltration capacity is not exceeded by the rainfall intensity. While in figure 5b it can be observed that there has been formed a

water table in the fill material (loose sand layer). Once the water front reached the interface between the two layers, a thin seepage layer was formed which started increasing upwards and more precisely from the toe towards the top due to the rainfall integration along the slope.

Only a small fraction was absorbed by the clay layer due to the large difference in the permeability values between the two layers: in fact the cohesive soil represents an unsaturated permeability barrier.

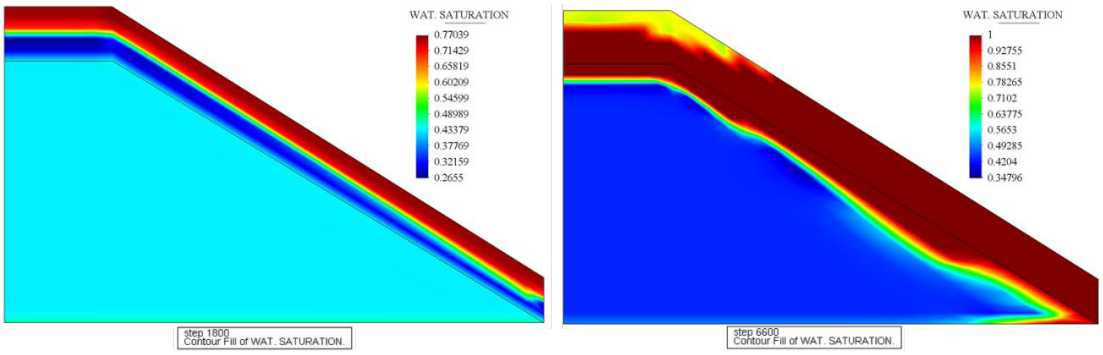

(a) (b)

Figure 5: Evolution of the wetting front (a) and the water table (b), during the rainfall infiltration.

The hydraulic response of the model is also depicted in Figure 6, through the volumetric water content time evolution at two different positions of the slope; at position 5 (TDR5) near the top of the sand layer and at position 6 (TDR6) near the interface between the two layers. The comparison is shown between the in-situ measurements and the prediction of the model. A two step evolution is noted: the water content increases from 0.18 to approximately 0.45 and subsequently it increases up again to 0.578. The first rise involves the probes from the top to the bottom while the second one progresses from the bottom to the top. As it can be observed the computed volumetric contents are in a good agreement with the field measurements.

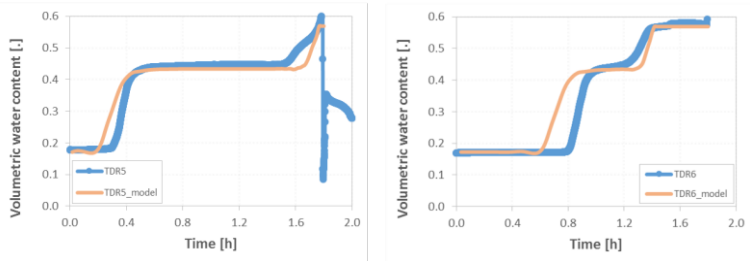

(a) (b)

Figure 6: Comparison between computed and in-situ measured volumetric water content at the positions 5 and 6 (TDR5 and TDR6 respectively).

The maximum displacements are concentrated on the upper surface near the toe, as illustrated in Figure 7. The vectors of the incremental displacements indicate that the sand is under swelling conditions at the end of the analysis because of the water overpressure and the constrained displacements at the toe. The equivalent plastic strain is also concentrated at the toe and coincides with the contours of the second order work (Figure 7c, 7d). The fact that the

maximum displacements contours coincide with the contour of the equivalent plastic strains and the second order work contour, indicates that the onset of the failure is located at the toe.

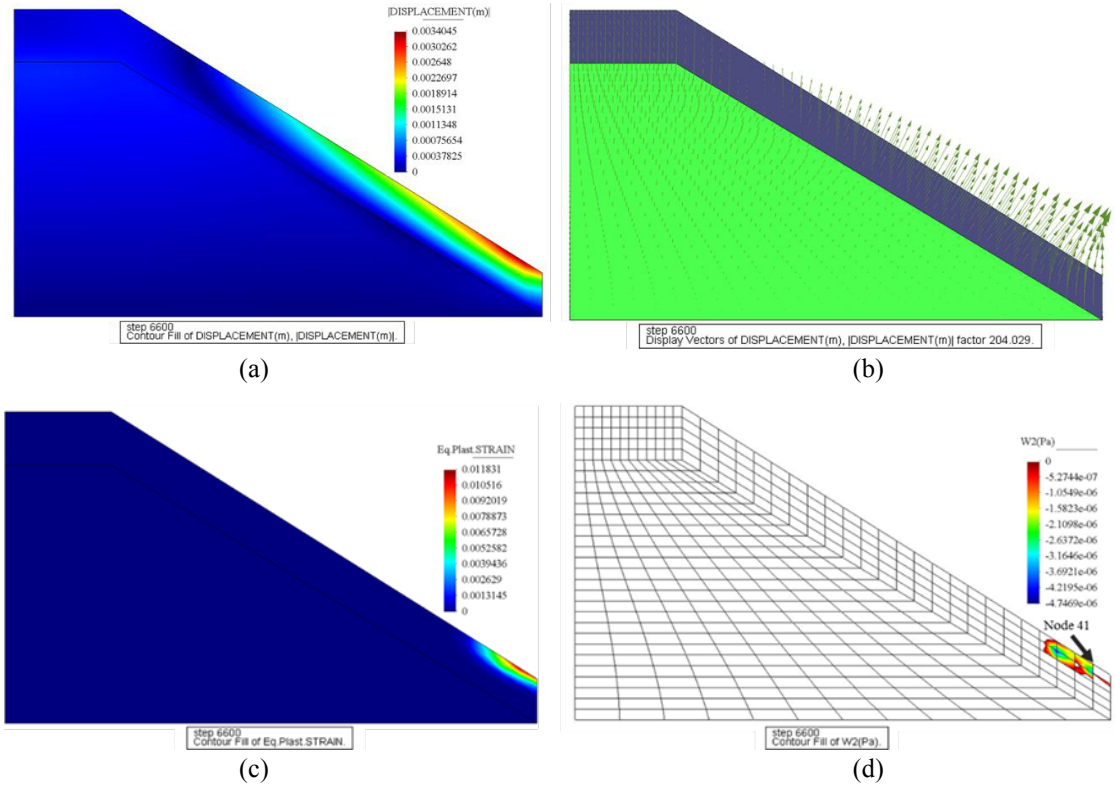

Figure 7: Displacement contours (a) and displacement vectors (b), equivalent plastic strain (c) and second order work contours (d), at the end of the analysis (after 1.8hr of rainfall input).

This is what is actually expected since it is the most sensitive point of the slope: there ends up all the seepage water within the layer and at the same time, it is being received the rainfall infiltration water as a flux input from the upper boundary surface. With increasing water content, the capillary forces acting between the soil particles decrease. This de-bonding effect of wetting is taken into account in the model through Schrefler's effective stress [22] $\boldsymbol{\sigma}' = \boldsymbol{\sigma} + \left[p^g - S^w p^c \right] \mathbf{1}$ which decreases during rain infiltration and as a consequence the soil loses its strength. When the point of significant excess pore water development is reached, there will be little or no effective confining stress acting on the soil. Eventually, the soil state approaches a zone of instability in which the shear strength can decrease significantly. Figure 8a, 8b describes exactly this phenomenon of a probable liquefaction occurrence, as it was captured, indicatively, on node 41 at the toe of the slope. Nearly at 1.5 hr the capillary pressure becomes negative (relative water pressure) and it is at that moment that the mean pressure starts to decrease until the 1.6 hr that becomes zero. At the same time, the deviatoric stress increases considerably and slightly after (1.7 hr) drops abruptly. At the moment of the peak deviatoric stress the equivalent plastic strain begins to develop and it is obtained the first negative value of the second order work at the material point level, as illustrated in Figure 8c.

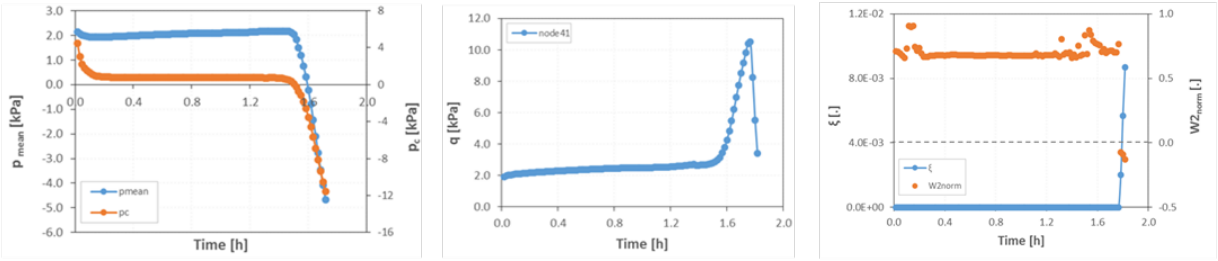

(a) (b) (c)

Figure 8: Evolution of: the capillary pressure and the mean stress (a); deviatoric stress (b); equivalent plastic strain and the second order work (c).

7 CONCLUSION

In this work, the modelling of rainfall-induced slope failure is considered as a coupled variably saturated hydro-mechanical problem. Therefore, a multiphase model for elasto-plastic porous media is used for the analysis of a large scale experimental test, in conjunction with a criterion based on the sign of the second-order work for the detection of instability. It is shown that multiphysics modelling of the initiation of flowslides can give results in a good agreement with the in-situ observations and can be a powerful tool for the better understanding of the triggering mechanisms that take place during the progressive failure. In particular, it is shown that the model can predict the field measurements of the volumetric water content and also provide us with the necessary mechanical results which indicate the liquefaction occurrence at the real time of the failure. The results taken from the second order work criterion at the material scale are in consistency with the mechanical response of the slope (results obtained from the equivalent plastic strain, mean and deviatoric stress) encouraging further research on this criterion.

ACKNOWLEDGEMENT

The authors would like to thank the 7th Framework Programme of the European Union (ITN MuMoLaDe project 289911) for the financial support.

REFERENCES

[1] Cascini, L., Cuomo, S., Pastor, M., Sorbino, G. Modeling of Rainfall-Induced Shallow Landslides of the Flow-Type. *Journal of Geotechnical and Geoenvironmental Engineering*, vol. 136, no. 1, pp. 85-98, 2010.

[2] Lewis, R. W., Schrefler, B. A. *The Finite Element Method in the Static and Dynamic Deformation and Consolidation of Porous Media*. Second. Chichester, UK: John Wiley & Sons, 1998.

[3] Gawin, D., Schrefler, B. A. Thermo-hydro-mechanical analysis of partially saturated porous materials. *Engineering Computations*, vol. 13, no. 7, pp. 113-143, 1996.

[4] Sanavia, L., Pesavento, F., Schrefler, B. A. Finite element analysis of non-isothermal multiphase geomaterials with application to strain localization simulation. *Computational Mechanics*, vol. 37, no. 4, pp. 331-348, May 2006.

[5] Sanavia, L., François, B., Bortolotto, R., Luison, L., Laloui, L. Finite element modelling of thermo-elasto-plastic water saturated porous materials. *Journal of Theoretical and Applied Mechanics*, vol. 38, no. 1-2, pp. 7-24, 2008.
[6] Sanavia, L. Numerical modelling of a slope stability test by means of porous media mechanics. *Engineering Computations*, vol. 26, no. 3, pp. 245 - 266, 2008.
[7] Hill, R. A general theory of uniqueness and stability in elastic-plastic solids. *Journal of the Mechanics and Physics of Solids*, vol. 6, no. 3, pp. 239-249, 1958.
[8] Schrefler, B. A. Mechanics and thermodynamics of saturated/unsaturated porous materials and quantitative solutions. *Applied Mechanics Reviews*, vol. 55, no. 4, pp. 351-388, 2002.
[9] Hassanizadeh, M., Gray, W. G. General conservation equations for multi-phase systems: 1. Averaging procedure. *Advances in Water Resources*, vol. 2, no. C, pp. 131-144, 1979.
[10] Hassanizadeh, M., Gray, W. G. General conservation equations for multi-phase systems: 3. Constitutive theory for porous media flow. *Advances in Water Resources*, vol. 3, no. 1, pp. 25-40, 1980.
[11] Darve, F. Stability and uniqueness in geomaterials constitutive modelling. *Localisation and bifurcation theory for soils and rocks*. Chambon, Desrues, and Vardoulakis, Eds. Balkema, 1994, pp. 73–88.
[12] Laouafa, F., Darve, F. Modelling of slope failure by a material instability mechanism. *Computers and Geotechnics*, vol. 29, no. 4, pp. 301-325, 2002.
[13] Darve, F., Servant, G., F., Laouafa, F., Khoa, H. D. V. Failure in geomaterials: continuous and discrete analyses. *Computer methods in applied mechanics and engineering*, vol. 193, no. 27-29, pp. 3057-3085, 2004.
[14] Nicot, F., Daouadji, A., Laouafa, F. Second-order work , kinetic energy and diffuse failure in granular materials. *Granular Matter*, vol. 13, no. 1, pp. 19-28, 2011.
[15] Lignon, S., Laouafa, F., Prunier, F., Khoa, H. D. V., Darve, F. Hydro-mechanical modelling of landslides with a material instability criterion. *Géotechnique*, vol. 59, no. 6, pp. 513-524, 2009.
[16] Lora, M. *Rainfall-triggered shallow landslides in a large-scale physical model*. Ph.D. Thesis, University of Padua, Padua (Italy), 2015.
[17] Lora, M., Camporese M., Salandin, P. Rainfall-triggered shallow landslides: infiltration dynamics in a physical hillslope model. *Submitted to Hydrological Processes*.
[18] Lora, M., Camporese M., Salandin, P. Design and Performance of a Nozzle Rainfall Simulator for Landslide Triggering Experiments. *Submitted to Cattena*.
[19] Brooks, R. H., Corey, A. T. Hydraulic properties of porous media. *Hydrology Papers*, vol. 3, no. 3, p. 27, 1964.
[20] Van Genucchten, M. T. A closed-form equation for predicting the hydraulic conductivity of unsaturated soils. *Soil Science Society of America Journal*, vol. 44, no. 5, pp. 892-898, 1980.
[21] Carsel, R. F., Parrish, R. S. Developing joint probability distributions of soil water retention characteristics. *Water Resources*, vol. 24, pp. 755-769, 1988.
[22] Schrefler, B. A. *The finite element method in soil consolidation (with applications to surface subsidence)*. Ph.D. Thesis, University College of Swansea, C/Ph/76/84, Swansea (UK), 1984.